



## Demonstration of AlGa<sub>N</sub>-based Far-UVC LED Epitaxial Growth by Using SR4000HT and Development of Technology to Improve Uniformity by Controlling Al Composition and Thickness of AlGa<sub>N</sub>

YOSHINAGA Junya\* IKEJIRI Keitaro\* TOKUNAGA Hiroki\*  
 KOSEKI Shuichi\* JO Masafumi\*\* HIRAYAMA Hideki\*\*

Far-UVC light with a wavelength of 200-230 nm has been shown to inactivate viruses without adversely affecting the human body, and there are high expectations for its practical application as a virus inactivation technology that can be used in a manned environment. The SR4000HT metal organic chemical vapor deposition (MOCVD) system of Taiyo Nippon Sanso Corp. has demonstrated the luminescence of aluminum gallium nitride (AlGa<sub>N</sub>)-based deep ultraviolet light-emitting diodes (UVC LEDs) in the 280-nm band, there was a problem of not being able to demonstrate the luminescence at shorter wavelengths. In this development, we worked on the epitaxial growth technology development of AlGa<sub>N</sub>-based Far-UVC LEDs using the SR4000HT. By adjusting the supply rate of metal organic, the Al composition of the AlGa<sub>N</sub> layer that constitutes the LED structure could be linearly controlled. Using this Al composition control technique, a UVC LED emitting at a wavelength of 226 nm was successfully fabricated. The peak emission wavelength was distributed between 227.8 and 229.1 nm in the wafer diameter direction, and a wavelength uniformity of Max-Min=1.3 nm was obtained. The control of the in-plane Al composition distribution and film thickness distribution in the AlGa<sub>N</sub> layer was confirmed to be easy. These results indicate that the SR4000HT is suitable for improving the in-plane wafer uniformity of Al composition and thickness, which contribute to optical output and emission wavelength.

### 1. Introduction

The spread of severe acute respiratory syndrome coronavirus 2 (SARS-CoV-2), which is the cause of novel coronavirus infection (COVID-19), poses a serious threat to human health worldwide. As a direct method to prevent SARS-CoV-2 and other viral infections, the virus inactivation effect of deep ultraviolet (UVC) light irradiation has been demonstrated<sup>1-3)</sup>. However, conventional mercury lamps with a wavelength of 254 nm and deep ultraviolet light-emitting diodes (UVC LEDs) with a wavelength of 260 to 280 nm have a potential to cause cancer or cataract and their widespread use in the public environment has been limited.

On the other hand, it has been shown that far-ultraviolet (Far-UVC) light with a wavelength of 220 nm band is harmless even when irradiated on mammalian skin and efficiently inactivates bacteria. This is because Far-UVC light cannot penetrate the outer layers of human skin and eyes due to its strong absorption by biological substances, but can penetrate the outer membrane of viruses of micrometer or

smaller size<sup>4-11)</sup>.

Although the practical application of ultraviolet light irradiators with a wavelength of 222 nm using excimer lamps as Far-UVC light sources is being proceeded with, it is eagerly awaited to replace them with LEDs in terms of power consumption, durability, and safety, just as fluorescent and incandescent lamps have been replaced with LEDs so far<sup>10)</sup>.

Gallium nitride (Ga<sub>N</sub>) and aluminum nitride (Al<sub>N</sub>) are wide bandgap semiconductors with a wide forbidden energy gap of 3.5 eV and 6.3 eV, respectively. UVC LEDs using aluminum gallium nitride (AlGa<sub>N</sub>), a mixture of Al<sub>N</sub> and Ga<sub>N</sub>, are expected as one of the next-generation UVC light sources because the emission of light with a wavelength of 210 to 320 nm can be freely controlled by the Al composition in AlGa<sub>N</sub><sup>12-24)</sup>. AlGa<sub>N</sub>-based Far-UVC LEDs with light output exceeding 1 mW at a wavelength of 228 nm have already been reported, and early social implementation of virus inactivation equipment that can be used in an environment where people are present is expected to be realized for entire public spaces such as a waiting room in a hospital<sup>25)</sup>.

\* Taiyo Nippon Sanso Corporation, CSE Department, Innovation Unit

\*\* Institute of Physical and Chemical Research (Riken)

However, in such Far-UVC wavelength range, the optical output and external quantum efficiency (EQE) are significantly reduced<sup>26-30</sup>. In addition, in the epitaxial growth of Far-UVC LEDs, it is very important to improve the uniformity of the in-plane distribution of light output and emission wavelength from the viewpoint of yield in mass production.

This report describes EL emission at an emission wavelength of 226 nm using a technique for controlling the Al composition in the AlGaIn well layer that constitutes the LED structure, and also describes a technique for improving the in-plane uniformity of the Al composition and the film thickness of the AlGaIn well layer that contributes to uniformity in the optical output and emission wavelength distribution.

## 2. Features of SR4000HT

In this development, our SR4000HT metal organic chemical vapor deposition (MOCVD) equipment was used. This equipment was developed for the production of UVC LEDs based on our conventional SR4000. The equipment is capable of handling three 2-inch substrates or one 4-inch substrate, and suitable for research and development, small-lot production, and pre-production evaluation testing.

Figure 1 shows a schematic diagram of the reactor of this equipment. The main feature of this reactor is its capability that allows epitaxial growth at 1350°C, 150°C higher than the conventional SR4000. It has the same three-layer gas flow in the lateral direction and two-zone split heater as the SR4000.

Epitaxial growth of AlGaIn-based Far-UVC LEDs requires high Al composition in order to shorten the wavelength. To minimize lattice mismatch with high-Al-composition AlGaIn as much as possible, AlN is commonly used as a template<sup>13,17</sup>. To grow AlN with high crystallinity, a high-temperature environment is needed in order to promote surface diffusion of Al atoms and Al free radicals<sup>31-38</sup>. As mentioned above, the SR4000HT is capable of high-temperature growth and is suitable for high-quality epitaxial growth of AlN.

On the other hand, as the temperature rises, gas-phase pre-parasitic reactions such as adduct formation by trimethylaluminum (TMAI) and ammonia (NH<sub>3</sub>) occur<sup>39-41</sup>. These parasitic reactions not only cause wastage of raw material gas, but also seriously affect epitaxial growth, such as unintended impurity doping, reduction of growth uniformity, and generation of dislocations<sup>35-38</sup>.

To address this issue, a lateral three-layer gas flow system that separates the gas nozzle supplying the Group III material and the gas nozzle supplying the Group V material is effective. This system, which is also used in SR4000, supplies the Group III material TMAI and the Group V material NH<sub>3</sub> at a lower temperature while keeping them separate until the heating region is reached, thereby suppressing parasitic reactions<sup>37</sup>.

The heater of this equipment consists of two zones, inner and outer, and the output ratio of each heater can be changed to control the in-plane temperature distribution of the susceptor. Furthermore, each of the top, middle, and bottom nozzles of the lateral three-layer gas flow described above can independently adjust the carrier gas flow rate. With these two functions, it is possible to control the region of gas-phase reaction of the material.

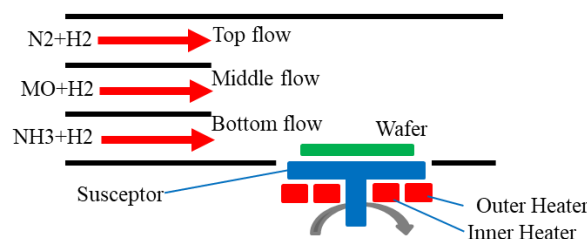


Figure 1 Schematic diagram of reactor of SR4000HT

## 3. Template substrate and materials used

We used a 2-inch c-plane (0001) sapphire substrate on which 3 μm AlN was grown by SR4000HT as the template substrate. The AlN template substrates were well crystalline, where the full widths at half maximum (FWHM) of the (0002) plane and (10-12) plane was approximately 150 arcsec and 350 arcsec, respectively, as measured by ω-scan of X-ray diffraction (XRD), which is an index of crystallinity.

Trimethylgallium (TMGa), TMAI, NH<sub>3</sub>, monosilane (SiH<sub>4</sub>), and bis-cyclopentadienylmagnesium (Cp<sub>2</sub>Mg) were used as the supply sources for gallium (Ga), aluminum (Al), nitrogen (N), silicon (Si), and magnesium (Mg), respectively. Hydrogen gas (H<sub>2</sub>) and nitrogen gas (N<sub>2</sub>) were used as carrier gases.

## 4. Control of Al composition in AlGaIn layer

Figure 2 shows the structure of AlGaIn, which consists of

a 480 nm AlN layer and a 100 nm AlGaIn layer. The reactor pressure was 30 kPa and the growth temperature was 1140°C. The ratio of TMAI to the sum of TMAI and TMGa was defined as the TMAI supply ratio, and by adjusting the amount of TMGa supply, the TMAI supply ratio (TMAI/(TMAI+TMGa)) was changed from 0.66, 0.73, to 0.82, to grow AlGaIn layers. The growth time was adjusted to obtain a constant film thickness of AlGaIn with any of the three TMAI supply ratios. The Al composition in the AlGaIn layer in each sample was measured by using XRD 2θ-ω scans.

Figure 3 shows the relationship between the TMAI supply ratio and the Al composition in AlGaIn. It was confirmed that the Al composition in AlGaIn changed linearly with the TMAI supply ratio in a high-Al composition region from 0.81 to 0.91. This indicates that the parasitic reaction between TMAI and NH<sub>3</sub> can be suppressed even in the case of high-Al compositions. This is considered to be an effect of the system that keeps TMAI (Group III material) and NH<sub>3</sub> (Group V material) separate and supplies them at a low temperature until the heating region is reached.

The fact that the Al composition in AlGaIn is higher compared to the TMAI supply ratio is thought to be due to the evaporation of Ga in the gas phase due to growth at higher temperatures and the resultant reduction in the Ga component in the solid phase<sup>42)</sup>.

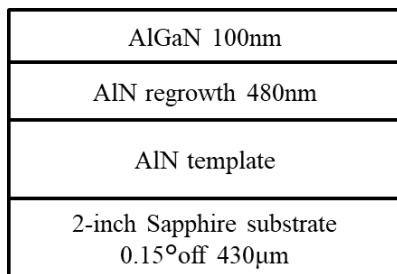


Figure 2 Structure of AlGaIn

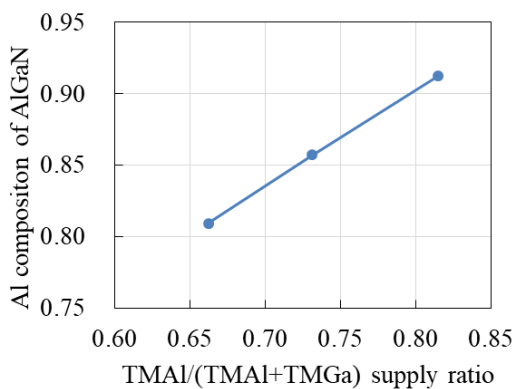


Figure 3 Relationship between TMAI supply ratio and Al composition in AlGaIn

## 5. Controllability and in-plane uniformity of Far-UVC LED emission wavelength

Figure 4 shows the structure of the UVC LED employed in this development. The multiple quantum well (MQW) structure of the UVC LED consists of an 8.8 nm Si-doped AlGaIn barrier layer and a 1.7 nm AlGaIn well layer in three periods.

As the initial conditions for the growth of the AlGaIn layers comprising the MQW, the reactor pressure was set to 30 kPa, the growth temperature to 1140°C, the inner heater power adjustment to 80%, the outer heater to inner heater ratio to 95%, and the carrier gas flow conditions for the top (T), middle (M), and bottom (B) of the lateral three layers to 25, 25, and 25 SLM. With these conditions fixed, the TMAI supply ratio (TMAI/(TMAI+TMGa)) of the AlGaIn well layer was set to 0.29, 0.48, 0.57, 0.62, 0.67, and 0.69 to shorten the UVC LED wavelengths. Other conditions such as reactor pressure, growth temperature, and carrier gas flow rate for each layer were set by comparing the conditions under which UVC LED luminescence can be obtained.

On the post-epitaxial growth substrate, a p-electrode of 400 × 400 μm<sup>2</sup> size was formed by alloying annealing under 500°C for 5 minutes in N<sub>2</sub> atmosphere after deposition of 20 nm nickel (Ni) / 100 nm gold (Au). n-electrode was formed by crimping indium (In). By using a monochromator and a silicon (Si) charge-coupled device (CCD), electroluminescence (EL) spectra from the UVC LED upon injection of 20 mA current were measured at three points in the wafer radial direction.

Figure 5 shows the EL spectra of the UVC LED. Short wavelength band edge emission from MQW up to 226 nm was obtained by increasing the TMAI supply ratio during the growth of the AlGaIn well layers in the MQW. 226 nm EL spectrum had a FWHM of approximately 10 nm.

Figure 6 shows the relationship between the TMAI supply ratio and the EL peak wavelength of the UVC LED. It is confirmed that the wavelength is linearly shortened as the TMAI supply ratio is increased. This result indicates that the emission wavelength can be easily adjusted by the TMAI supply ratio.

Figure 7 shows the measured positions of the EL spectra, and Figure 8 shows the EL spectra of the Far-UVC LED at the three measurement positions. The EL peak wavelength was distributed between 227.8 and 229.1 nm in the wafer diameter direction, with a wavelength uniformity of

Max - Min = 1.3 nm. The in-plane distribution of Al composition in AlGa<sub>N</sub> was Max - Min = 0.010, and the in-plane distribution of film thickness was (Max - Min)/Average = 7.4%.

p-GaN 50nm
p-AlGa <sub>N</sub> 50nm
AlGa <sub>N</sub> or AlN EBL 10nm
AlGa <sub>N</sub> last barrier 8.8nm
AlGa <sub>N</sub> -MQW (3-pair) well 1.7nm
Si-doped barrier 8.8nm
Middle-AlGa <sub>N</sub> :Si 70nm
n-AlGa <sub>N</sub> :Si 2μm
ud-AlGa <sub>N</sub> 300nm
AlN regrowth 480nm
AlN template
2-inch Sapphire substrate 0.15°off 430μm

Figure 4 Structure of UVC LED employed in this development

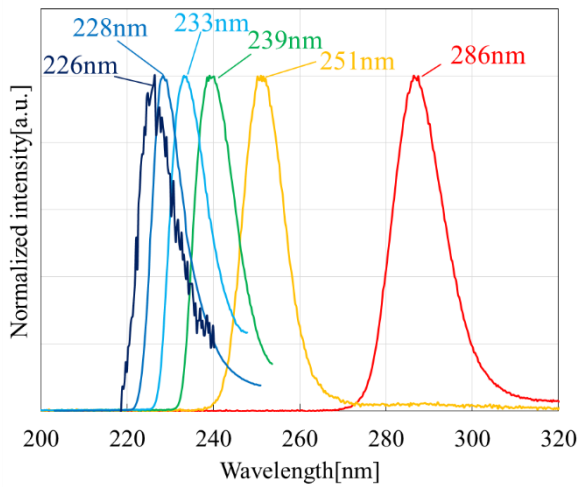


Figure 5 EL spectra of UVC LED

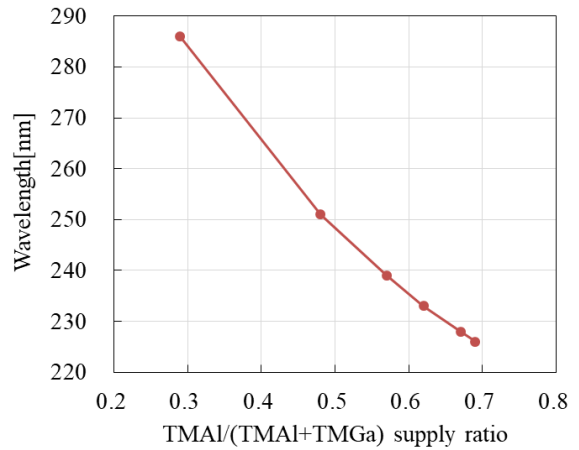


Figure 6 Relationship between TMAI supply ratio and EL peak wavelength of UVC LED

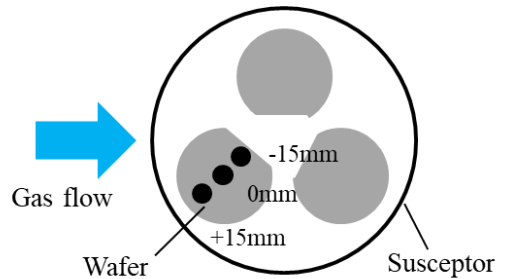


Figure 7 Measurement positions of EL spectrum

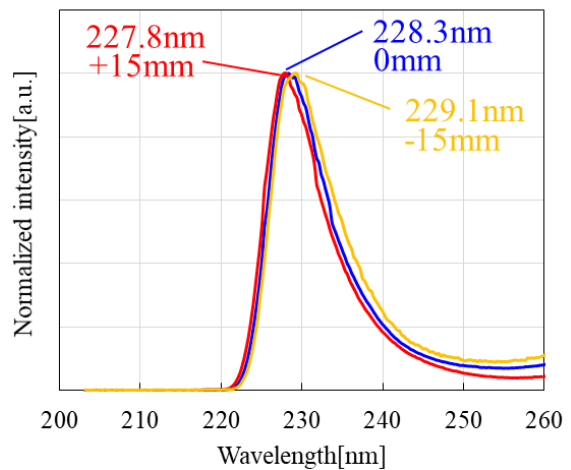


Figure 8 EL spectra of Far-UVC LEDs at three measurement positions

### 6. In-plane uniformity control of Al composition and film thickness of AlGaIn layer

In AlGaIn layers, the effects of various growth parameters on (1) the dependence of Al composition on heater power ratio, (2) the dependence of film thickness on total carrier gas flow rate, and (3) the dependence of film thickness on carrier gas flow balance are considered.

Based on the growth conditions for the AlGaIn well layer of the Far-UVC LED described in the previous section, the AlGaIn structure consisting of a 480 nm AlN layer and a 100 nm AlGaIn layer shown in Figure 2 was grown. The reactor pressure was set at 30 kPa and the growth temperature was set at 1140°C. The Al composition and film thickness of the AlGaIn layer were measured at three points in the wafer radial direction for each sample by XRD 2θ-ω scanning. Figure 9 shows the XRD 2θ-ω scan measurement positions.

First, the inner heater output adjustment was set to 80%, and the output ratio of the outer heater to inner heater was varied to 91%, 93%, and 95% to check the effect on the Al composition in the AlGaIn layer. Figure 10 shows the relationship between the heater output ratio and the Al composition in AlGaIn. When the output ratio of the outer heater to inner heater was decreased, the Al composition in the AlGaIn layer at the measurement position "+20 mm" decreased. This is assumed to be because lowering the output ratio of the outer heater to inner heater lowers the temperature outside the susceptor, making it difficult for AlN, which requires higher temperature for crystal growth than GaN, to contribute to the AlGaIn layer. The Al composition uniformity lowered to the lowest with Max - Min = 0.004 when the inner heater output adjustment was 80% and the output ratio of the outer heater to inner heater was 91%.

Next, the total flow rate of the carrier gas was varied to 75, 90, and 105 SLM to check the effect on the film thickness of the AlGaIn layer. Figure 11 shows the relationship between the total carrier gas flow rate and the film thickness of the AlGaIn layer. The film thickness of the AlGaIn layer at the measurement position "+20 mm" became thinner as the total flow rate of the carrier gas was increased, and the uniformity of the film thickness of the AlGaIn layer lowered to the smallest with (Max - Min)/Average = 2.7% when the total flow rate of the carrier gas was 105 SLM. This is considered to be because the gas-phase reaction region was moved as a result of increasing the total flow rate of the carrier gas.

Finally, the top-middle-bottom carrier gas flow rate balance was varied from 25-25-25, 23-26-26, and 21-27-27 SLM to check the effect on the film thickness of the AlGaIn layer. Figure 12 shows the relationship between the carrier gas flow rate balance and the film thickness of the AlGaIn layer. The film thickness of the AlGaIn layer at the measurement position "+20 mm" became thinner as the top carrier gas flow ratio was decreased, as was the case when the total carrier gas flow rate was increased. The film thickness uniformity in the AlGaIn layer lowered to the smallest with (Max - Min)/Average = 3.0% when the top-middle-bottom carrier gas flow rate was 23-26-26 SLM. This is considered to be because the gas-phase reaction region was moved as a result of decreasing the ratio of the top carrier gas flow rate.

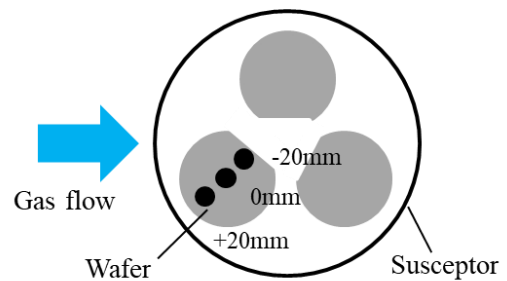


Figure 9 XRD 2θ-ω scan measurement positions

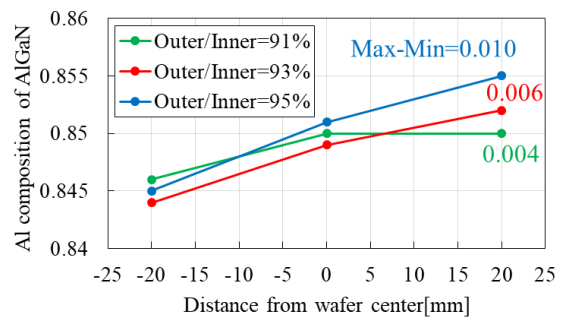


Figure 10 Relationship between heater output ratio and Al composition in AlGaIn layer

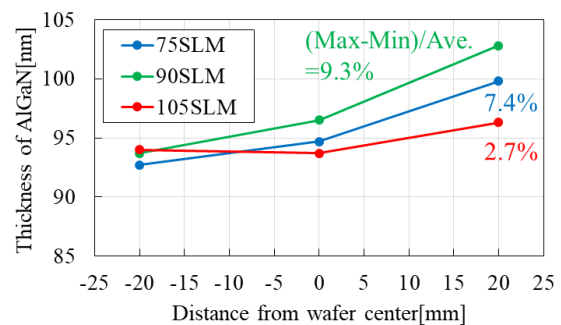


Figure 11 Relationship between total flow rate of carrier gas and film thickness of AlGaIn layer

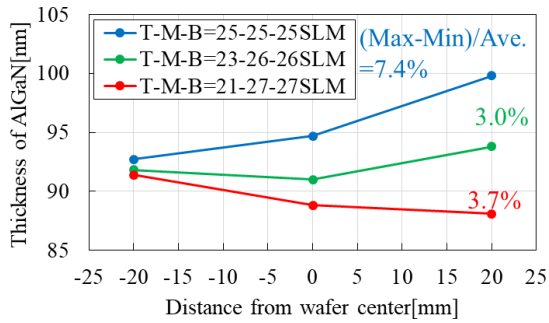


Figure 12 Relationship between carrier gas flow rate balance and film thickness of AlGaIn layer

## 7. Conclusion

It was confirmed that the Al composition in the AlGaIn layer changed linearly in the high Al composition region from 0.81 to 0.91 with respect to the supply rate of TMAI and TMGa ( $TMAI / (TMAI + TMGa)$ ) using our MOCVD equipment SR4000HT. This result shows that the parasitic reaction between TMAI and  $NH_3$  can be suppressed even with high Al compositions.

Since the wavelength of the UVC LED becomes shorter as the Al composition in the AlGaIn layer increases, we succeeded in shortening the EL peak wavelength to the 220 nm band through the realization of this AlGaIn layer with high Al composition. This result indicates that the EL emission wavelength can be easily adjusted by adjusting the amount of TMAI and other materials supplied.

The EL peak wavelength was distributed between 227.8 and 229.1 nm in the wafer radial direction, and a wavelength uniformity of  $Max - Min = 1.3$  nm was obtained. The in-plane distribution of Al composition in the AlGaIn well layer of the MQW at that time was  $Max - Min = 0.010$ , and the in-plane distribution of film thickness was  $(Max - Min) / Average = 7.4\%$ .

Finally, it was confirmed that the in-plane Al composition distribution of the AlGaIn layer can be controlled by adjusting the output power of the two-zone split heater under the growth conditions of the AlGaIn well layer. The minimum value of the in-plane Al composition distribution was  $Max - Min = 0.004$ .

It was confirmed that the in-plane film thickness distribution of the AlGaIn layer can be controlled by adjusting the total carrier gas flow rate and the gas flow

rate balance of the lateral triple-layer gas flow. The minimum in-plane film thickness distribution was  $(Max - Min) / Average = 2.7\%$ .

These results indicate that SR4000HT, which has a two-zone split heater and lateral triple-layer gas nozzles, can easily control the in-plane Al composition distribution and film thickness distribution of the AlGaIn layer, and is suitable for improving uniformity in the production of Far-UVC LEDs.

## References

- 1) Y. Gerchman, H. Mamane, N. Friedman, and M. Mandelboim, *J. Photochem. Photobiol. B.* 212, 112044(2020).
- 2) A. Gidari, S. Sabbatini, S. Bastianelli, S. Pierucci, C. Busti, D. Bartolini, A. M. Stabile, C. Monari, F. Galli, M. Rende, G. Cruciani, and D. Francisci, *Viruses.*, 13(3), 408(2021).
- 3) H. Shimoda, J. Matsuda, T. Iwasaki, and D. Hayasaka, *J. Photochem. Photobiol.* 7, 100050(2021).
- 4) N. Yamano, M. Kunisada, S. Kaidzu, K. Sugihara, A. Nishiaki-Sawada, H. Ohashi, A. Yoshioka, T. Igarashi, A. Ohira, M. Tanito, and C. Nishigori, *Photochem. Photobiol.* 96(4), 853(2020).
- 5) M. Buonanno, D. Welch, I. Shuryak, and D. J. Brenner, *Sci. Rep.* 10(1), 10285(2020).
- 6) K. Narita, K. Asano, K. Naito, H. Ohashi, M. Sasaki, Y. Morimoto, T. Igarashi, and A. Nakane, *J. Hosp. Infect.* 105(3), 459(2020).
- 7) W. Taylor, E. Camilleri, D. L. Craft, G. Korza, M. R. Granados, J. Peterson, R. Szczepaniak, S. K. Weller, R. Moeller, T. Douki, W. W. K. Mok, and P. Setlow, *Appl. Environ. Microbiol.* 86(8), e03039-19(2020).
- 8) D. Welch, M. Buonanno, V. Grilji, I. Shuryak, C. Crickmore, A. W. Bigelow, G. Randers-Pehrson, G. W. Johnson, and D. J. Brenner, *Sci. Rep.* 8(1), 2752(2018).
- 9) H. Kitagawa, T. Nomura, T. Nazmul, K. Omori, N. Shigemoto, T. Sakaguchi, and H. Ohge, *Am. J. Infect. Control* 49(3), 299(2021).
- 10) T. Fukui, T. Niikura, T. Oda, Y. Kumabe, H. Ohashi, M. Sasaki, T. Igarashi, M. Kunisada, N. Yamano, K. Oe, T. Matsumoto, T. Matsushita, S. Hayashi, C. Nishigori, and R. Kuroda, *PLoS One* 15, e0235948(2020).
- 11) S. Kaidzu, K. Sugihara, M. Sasaki, A. Nishiaki, T. Igarashi, and M. Tanito, *Free Radical Res.* 53(6), 611(2019).
- 12) H. Hirayama, *J. Appl. Phys.* 97, 091101(2005).
- 13) H. Hirayama, S. Fujikawa, N. Noguchi, J. Norimatsu, T. Takano, K. Tsubaki, and N. Kamata, *Phys. Status Solidi A* 206, 6, 1176-1182(2009).
- 14) H. Hirayama, T. Yatabe, N. Noguchi, T. Ohashi, and N. Kamata, *Appl. Phys. Lett.* 91, 071901 (2007).
- 15) H. Hirayama, N. Noguchi, T. Yatabe, and N. Kamata, *Appl. Phys. Express* 1, 051101 (2008).
- 16) H. Hirayama, Y. Enomoto, A. Kinoshita, A. Hirata, and Y. Aoyagi, *Appl. Phys. Lett.* 80, 37 (2002).
- 17) M. Jo, N. Maeda, and H. Hirayama, *Appl. Phys. Express* 9, 012102(2016).
- 18) Y. Kashima, N. Maeda, E. Matsuura, M. Jo, T. Iwai, T. Morita, M. Kokubo, T. Tashiro, R. Kamimura, Y. Osada, *Appl. Phys. Express* 11, 012101(2018).
- 19) C. Pernot, M. Kim, S. Fukahori, T. Inazu, T. Fujita, Y. Nagasawa, A. Hirano, M. Ippommatsu, M. Iwaya, and S. Kamiyama, *Appl. Phys. Express* 3(6), 061004(2010).
- 20) M. Shatalov, W. Sun, A. Lunev, X. Hu, A. Dobrinsky, Y. Bilenko, J. Yang, M. Shur, R. Gaska, and C. Moe, *Appl. Phys. Express* 5(8), 082101(2012).
- 21) J. Grandusky, J. Chen, S. R. Gibb, M. C. Mendrick, C. G. Moe, L. Rodak, G. A. Garrett, M. Wraback, and L. J. Schowalter, *Appl. Phys. Express* 6, 032101(2013).
- 22) A. Fujioka, T. Misaki, T. Murayama, Y. Narukawa, and T. Mukai, *Appl. Phys. Express* 3(4), 041001(2010).
- 23) T. Kinoshita, T. Obata, T. Nagashima, H. Yanagi, B. Moody, S. Mita, S. Inoue, Y. Kumagai, A. Koukitu, and Z. Sitar, *Appl. Phys. Express* 6(9), 092103(2013).
- 24) N. Lobo-Ploch, F. Mehnke, L. Sulmoni, H. K. Cho, M. Guttmann, J. Glaab, K. Hilbrich, T. Wernicke, S. Einfedt, and M. Kneissl, *Appl. Phys. Lett.* 117, 111102(2020).
- 25) M. Jo, Y. Itokazu, and H. Hirayama, *Appl. Phys. Lett.* 120, 211105(2022).
- 26) A. Yoshikawa, R. Hasegawa, T. Morishita, K. Nagase, S. Yamada, J. Grandusky, J. Mann, A. Miller, and L. J. Schowalter, *Appl. Phys. Express* 13, 022001(2020).
- 27) R. G. Banal, M. Funato, and Y. Kawakami, *Phys. Rev. B* 79(12), 121308 (2009).
- 28) C. Reich, M. Guttmann, M. Feneberg, T. Wernicke, F. Mehnke, C. Kuhn, J. Rass, M. Lapeyrade, S. Einfedt, A. Knauer, V. Kueller, M. Weyers, R. Goldhahn, and M. Kneissl, *Appl. Phys. Lett.* 107(14), 142101(2015).
- 29) S.-H. Park and Jong-In Shim, *Appl. Phys. Lett.* 102(22), 221109(2013).
- 30) M. Guttmann, F. Mehnke, B. Belde, F. Wolf, C. Reich, L. Sulmoni, T. Wernicke, and M. Kneissl, *JJAP* 58, SCCB20(2019).
- 31) K. Nagamatsu, S. Tsuda, T. Miyagawa, R. Aono, H. Hirayama, Y. Takashima, and Y. Naoi, *scientific reports.* 12, 7662(2022).
- 32) K. Tsujisawa, S. Kishino, Y. H. Liu, H. Miyake, K. Hiramatsu, T. Shibata, and M. Tanaka., *solid state physics*, 4(7), 2252-2255(2007).
- 33) M. E. Coltrin, J. R. Creighton, and C. C. Mitchell, *J. Cryst. Growth* 287(2), 566-571(2006).
- 34) J. An, L. Feng, and J. Zheng, *Sci Rep.*, 11(1), 8877(2021).
- 35) J. An, X. Dai, Q. Zhang, R. Guo, and L. Feng, *ACS Omega* 5(20), 11792-11798 (2020).
- 36) H. Zhang, R. Zuo, T. Zhong, and L. Zhang, *J. Phys. Chem. A* 124, 2961-2971(2020).
- 37) K. Matsumoto and A. Tachibana, *J. Cryst. Growth* 272, 360-369 (2004).
- 38) T. G. Mihopoulos, V. Gupta, and K. F. Jensen, *J. Cryst. Growth* 195, 733-739 (1998).
- 39) J. Leitner, J. Stejskal, and Z. Sofer, *phys. Stat. sol. c* 0(1), 133-136(2002).
- 40) D. G. Zhao, J. J. Zhu, D. S. Jiang, H. Yang, J. W. Liang, X. Y. Li, and H. M. Gong, *J. Cryst. Growth* 289(1), 72-75(2006).
- 41) K. Pu, X. Dai, D. Miao, S. Wu, T. Zhao, Y. Hao, *J. Cryst. Growth* 478, 42-46(2017).
- 42) A. Bchetnia, I. Kemis, A. Toure, W. Fathallah, T. Boufaden, and B. E. Jani, *Semicond. Sci. Technol.* 23, 125025(2008).